9380 *Inorg. Chem.* **2010**, *49*, 9380–9391
DOI: 10.1021/ic101077t

Inorganic Chemistry
Article

Iron(II) and Ruthenium(II) Complexes Containing P, N, and H Ligands: Structure, Spectroscopy, Electrochemistry, and Reactivity

Jinzhu Chen,[†] David J. Szalda,[‡] Etsuko Fujita,[†] and Carol Creutz*[,†]

[†]*Chemistry Department, Brookhaven National Laboratory, Upton, New York 11973-5000, and*
[‡]*Department of Natural Sciences, Baruch College, New York, New York 10010*

Received May 27, 2010

The purpose of this work was to explore the possibility of using iron(II) hydrides in CO_2 reduction and to compare their reactivity to that of their ruthenium analogues. $Fe(bpy)(P(OEt)_3)_3H^+$ and $Ru(bpy)(P(OEt)_3)_3H^+$ do not react with CO_2 in acetonitrile, but the one-electron-reduction products of $Ru(bpy)(P(OEt)_3)_3H^+$ and $Ru(bpy)_2(P(OEt)_3)H^+$ and the two-electron-reduction product of $Fe(bpy)(P(OEt)_3)_3H^+$ do. $Ru(bpy)_2(P(OEt)_3)H^+$ also reacts slowly with CO_2 to give a formate complex [as reported previously by Albertin et al. (*Inorg. Chem.* **2004**, *43*, 1336)] with a second-order rate constant of $\sim 4 \times 10^{-3}$ M^{-1} s^{-1} in methanol. The structures for the hydride complexes $[Fe(bpy)(P(OEt)_3)_3H]^+$ and $[Ru(bpy)_2(P(OEt)_3)H]^+$ and for the (η^5-Cp)bis- and -tris-PTA complexes (PTA = 1,3,5-triaza-7-phosphatricyclo-[3.3.1.13.7]decane) of iron(II) are reported. These and the $CpFe(CO)(bpy)^+$ and Fe^{II}PNNP compounds have been subjected to electrochemical and UV−vis spectroscopic characterization. $Fe(bpy)(P(OEt)_3)_3H^+$ exhibits a quasi-reversible oxidation at +0.42 V vs AgCl/Ag in acetonitrile; $Ru(bpy)(P(OEt)_3)_3H^+$ and $Ru(bpy)_2(P(OEt)_3)H^+$ are oxidized irreversibly at +0.90 and +0.55 V, respectively, vs AgCl/Ag. The reduction site for $Fe(bpy)(P(OEt)_3)_3H^+$ and $Fe(bpy)(P(OEt)_3)_3(CH_3CN)^{2+}$ appears to be the metal and gives rise to a two-electron process. The bpy-centered reductions are negatively shifted in the ruthenium(II) hydride complexes, compared to the acetonitrile complexes. The results of attempts to prepare other iron(II) hydrides are summarized.

Introduction

Earlier we reported the insertion of CO_2, CO, and CH_2O into the Ru−H bond of $Ru(terpy)(bpy)H^+$ in water[1] and measured the hydricities of $Ru(terpy)(bpy)H^+$ and $Ru(\eta^6\text{-}C_6Me_6)(bpy)(H)^+$ (terpy = 2,2′;6′,2″-terpyridine and bpy = 2,2′-bipyridine) in water.[2] The C_1 reductions, if operating catalytically in the presence of a solar or solar photoelectrochemical source of reducing equivalents, could be valuable for generating the liquid fuel methanol (MeOH) from water and waste CO_2. Recognizing that an abundant metal would be more desirable for this purpose than ruthenium, we set out to try to devise or discover iron complexes that might serve in this role.

While a number of metal complexes have proven effective in the conversion of H_2 and CO_2 to formic acid,[3] only a few iron complexes have been reported to reduce CO_2.[4−13] These include iron(I) corroles,[5] iron(0) porphyrins,[10,14] multiply ligand-reduced iron(II) complexes of 2,6-bis[1-(phenylimino)-ethyl]pyridine in *N*,*N*-dimethylformamide (DMF),[8] 19-electron Cp complexes,[12] and the electrogenerated iron(I) complex of 2,9-bis(2-hydroxyphenyl)-1,10-phenanthroline.[6] These examples involve organic solvents and catalytic species that are highly reduced at the metal center, at the ligand, or both. Iron hydride complexes do not appear to be intermediates in the above systems. The insertion of CO_2 into Fe−H bonds has only recently been reported for $Fe(dmpe)_2(H)_2$.[15,16] Utilization of iron complexes as catalysts for transfer hydrogenation suggests, however, that iron hydrides are active in

*To whom correspondence should be addressed. E-mail: ccreutz@bnl.gov.

(1) Creutz, C.; Chou, M. H. *J. Am. Chem. Soc.* **2007**, *129*, 10108–10109.
(2) Creutz, C.; Chou, M. H. *J. Am. Chem. Soc.* **2009**, *131*, 2794–2795.
(3) Jessop, P. G.; Joó, F.; Tai, C. C. *Coord. Chem. Rev.* **2004**, *248*, 2425–2442.
(4) Lu, C. C.; Saouma, C. T.; Day, M. W.; Peters, J. C. *J. Am. Chem. Soc.* **2007**, *129*, 4–5.
(5) Grodkowski, J.; Neta, P.; Fujita, E.; Mahammed, A.; Simkhovich, L.; Gross, Z. *J. Phys. Chem. A* **2002**, *106*, 4772–4778.
(6) Pun, S. N.; Chung, W. H.; Lam, K. M.; Guo, P.; Chan, P. H.; Wong, K. Y.; Che, C. M.; Chen, T. Y.; Peng, S. M. *J. Chem. Soc., Dalton Trans.* **2002**, 575–583.
(7) Grodkowski, J.; Dhanasekaran, T.; Neta, P.; Hambright, P.; Brunschwig, B. S.; Shinozaki, K.; Fujita, E. *J. Phys. Chem. A* **2000**, *104*, 11332–11339.
(8) Chiericato, G.; Arana, C. R.; Casado, C.; Cuadrado, I.; Abruna, H. D. *Inorg. Chim. Acta* **2000**, *300*, 32–42.
(9) Grodkowski, J.; Neta, P. *J. Phys. Chem. A* **2000**, *104*, 4475–4479.
(10) Grodkowski, J.; Behar, D.; Neta, P.; Hambright, P. *J. Phys. Chem. A* **1997**, *101*, 248–254.
(11) Fujita, E.; Creutz, C.; Sutin, N.; Szalda, D. J. *J. Am. Chem. Soc.* **1991**, *113*, 343–353.
(12) Ruiz, J.; Guerchais, V.; Astruc, D. *J. Chem. Soc., Chem. Commun.* **1989**, 812–813.
(13) Saveant, J.-M. *Chem. Rev.* **2008**, *108*, 2348–2378.
(14) Hammouche, M.; Lexa, D.; Momenteau, M.; Saveant, J. M. *J. Am. Chem. Soc.* **1991**, *113*, 8455–8466.
(15) Field, L. D.; Lawrenz, E. T.; Shaw, W. J.; Turner, P. *Inorg. Chem.* **2000**, *39*, 5632–5638.
(16) Hills, A.; Hughes, D. L.; Jimenez-Tenorio, M.; Leigh, G. J. *J. Organomet. Chem.* **1990**, *391*, C41–C44.

 Published on Web 09/21/2010

Chart 1

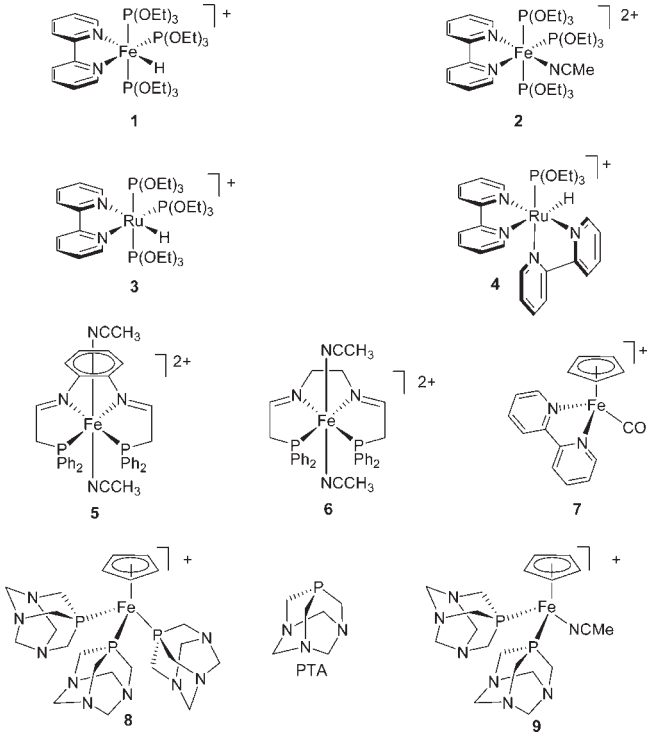

C=O reduction.[17−19] The catalysts are of two structural types: one is based on a PNNP chelate, and the other is based on a hydroxycyclopentadienideiron(II) hydride compound. Using these systems as inspiration, we set out to look for reactivity of iron(II) hydrides in water. We encountered many difficulties, especially obtaining pure hydrides and a good solubility in water, such that our limited results are mainly reported in the Supporting Information for this manuscript. We also examined the mixed phosphite and bpy complexes reported by Albertin et al.[20,21] Because the data bearing on the electronic structures of iron(II) in a number of ligand environments are sparse, we carried out electrochemical and electronic spectral measurements, mainly in an acetonitrile solvent. We characterized the reduced mixed phosphite and bpy complexes and surveyed their reactivity toward CO_2. Finding that the iron complexes are reduced at the metal while the ruthenium complexes are reduced at bpy, we used Lever's E_L model[22] to discuss this reactivity difference. Structures for the hydride complexes $[Fe(bpy)(P(OEt)_3)_3H](CF_3SO_3)$ and $[Ru(bpy)_2(P(OEt)_3)H](PF_6)$ and of (η^5-Cp)bis and -tris-PTA complexes (PTA = 1,3,5-triaza-7-phosphatricyclo[3.3.1.13.7]-decane) of iron(II) are reported.

Chart 1 shows the complexes prepared in this study, their numbering scheme, and the structure of PTA.

Experimental Section

General procedures. The redox potentials of the complexes were measured in an acetonitrile solution containing tetra-*n*-butylammonium hexafluorophosphate (0.1 M) as the supporting electrolyte. A BAS 100B electrochemical analyzer, with a glassy carbon working electrode, a AgCl (3 M)/Ag reference electrode, and a platinum counter electrode, was used. The supporting electrolyte was dried in vacuum prior to use. The experimental electrochemical potentials were measured using a AgCl/Ag reference electrode. They were converted to different reference electrodes using Chart 2.[23,24] UV−vis and IR absorption spectra were recorded on a Hewlett-Packard 8452A diode array spectrophotometer and a Thermo Nicolet NEXUS 690 FT-IR spectrometer, respectively. ^1H, $^{13}C\{^1H\}$, and $^{31}P\{^1H\}$ NMR spectra were recorded on a Bruker DRX-Avance 400 NMR spectrometer at 25 °C. Electrospray ionization mass spectrometry (ESI-MS) spectra were measured using a Thermo Finnigan LCQ Advantage mass spectrometer with an APCI probe. UV irradiations were performed by an Englehard−Hanovia water-cooled 450 W mercury lamp at room temperature.

Chart 2. Potentials of the Reference Electrodes (V)

Fc^+/Fc	+0.63
SCE	+0.25
AgCl/Ag	+0.20
NHE	0

Materials. All synthetic work was carried out under an appropriate atmosphere (Ar or N_2) using standard Schlenk techniques or a Vacuum Atmospheres drybox. Once isolated, the complexes were found to be relatively stable in air but were stored under an inert atmosphere. All solvents were dried over appropriate drying agents, degassed on a vacuum line, and distilled into vacuum-tight storage flasks. Triethyl phosphite (Aldrich) was purified by distillation under N_2. A potassium diphenylphosphide solution, bromoacetaldehyde diethyl acetal, $[Fe(H_2O)_6][BF_4]_2$, PTA, $[CpFe(CO)_2]_2$, and $NaBH_4$ were used as purchased from Aldrich without further purification.

The complexes $[Fe(bpy)(P(OEt)_3)_3(H)](CF_3SO_3)$,[21] $[Fe(bpy)(P(OEt)_3)_3(CH_3CN)](CF_3SO_3)_2$,[21] $Ru(bpy)Cl_4\cdot H_2O$,[25] $Ru(bpy)_2Cl_2\cdot 2H_2O$,[26] $[Ru(bpy)(P(OEt)_3)_3(H)](PF_6)$,[20] $[Ru(bpy)_2(P(OEt)_3)(H)](PF_6)$,[20] $[Fe(Ph_2PCH_2CH{=}N(C_6H_4)N{=}CHCH_2PPh_2)(CH_3CN)_2][BPh_4]_2$,[27,28] $Fe(bpy)Cl_2$,[29] $CpFe(CO)_2Cl$,[30] $[Fe(Ph_2PCH_2CH{=}NC_2H_4N{=}CHCH_2PPh_2)(CH_3CN)_2][BPh_4]_2$, and $[CpFe(CO)_2]I$[31] were prepared and identified as reported. The preparation and characterization of **7**−**9** are given in the Supporting Information.

We attempted to replace the tetraphenylborate anion in $\mathbf{6}[BPh_4]_2$ because it interferes with cyclic voltammetry (CV; see below). The sample of BF_4^- salt contained an impurity with a ^{31}P NMR resonance at 62.9 ppm.

When we attempted to prepare the hydride complexes of **5** and **6** by the reaction with $NaBH_4$ in CD_3CN, we found a reduction of the imine bonds.

We prepared an impure sample of $CpFe(PTA)_2(H)$ by treating **9** with $LiAlH_4$ in THF. Its ^1H NMR spectrum contained a peak attributable to Fe−H (triplet at δ −17.3 ppm). However, the $^{31}P\{^1H\}$ NMR spectrum with a main peak at 4.91 ppm exhibited impurity peaks between −8.1 and −15.7 ppm.

(17) Morris, R. H. *Chem. Soc. Rev.* **2009**, *38*, 2282–2291.
(18) Casey, C. P.; Guan, H. *J. Am. Chem. Soc.* **2007**, *129*, 5816–5817.
(19) Casey, C. P.; Guan, H. *J. Am. Chem. Soc.* **2009**, *131*, 2499–2507.
(20) Albertin, G.; Antoniutti, S.; Bacchi, A.; D'Este, C.; Pelizzi, G. *Inorg. Chem.* **2004**, *43*, 1336–1349.
(21) Albertin, G.; Antoniutti, S.; Bortoluzzi, M. *Inorg. Chem.* **2004**, *43*, 1328–1335.
(22) Lever, A. B. P. *Inorg. Chem.* **1990**, *29*, 1271–1285.
(23) Bard, A. J.; Faulkner, L. R. *Electrochemical Methods*, 2nd ed.; Wiley: New York, 2001.
(24) Pavlishchuk, V. V.; Addison, A. W. *Inorg. Chim. Acta* **2000**, *298*, 97–102.
(25) Krause, R. A. *Inorg. Chim. Acta* **1977**, *22*, 209–213.
(26) Sullivan, B. P.; Salmon, D. J.; Meyer, T. J. *Inorg. Chem.* **1978**, *17*, 3334–3341.
(27) Mikhailine, A. A.; Kim, E.; Dingels, C.; Lough, A. J.; Morris, R. H. *Inorg. Chem.* **2008**, *47*, 6587–6589.
(28) Matt, D.; Ziessel, R.; DeCian, A.; Fischer, J. *New J. Chem.* **1996**, *20*, 1257–1263.
(29) Broomhead, J. A.; Dwyer, F. P. *Aust. J. Chem.* **1961**, *14*, 250–252.
(30) Piper, T. S.; Cotton, F. A.; Wilkinson, G. *J. Inorg. Nucl. Chem.* **1955**, *1*, 165–174.
(31) Piper, T. S.; Wilkinson, G. *J. Inorg. Nucl. Chem.* **1956**, *2*, 38–45.

Table 1. Crystallographic Collection and Refinement Data for **1**, **4**, **8**, and **9**

	[Fe(bpy)(P(OEt)$_3$)$_3$H] (CF_3SO_3) (**1**CF_3SO_3)	[Ru(bpy)$_2$(P(OEt)$_3$)-H]PF_6 (**4**PF_6)	[Fe(Cp)(PTA)$_3$] $PF_6\cdot H_2O$ (**8**$PF_6\cdot H_2O$; PTA = $PC_6N_3H_{12}$)	[Fe(Cp)(PTA)$_2$ ($NCCH_3$)]-B(Ph)$_4\cdot HOCH_3$ (**9**B(Ph)$_4\cdot$ $HOCH_3$; PTA = $PC_6N_3H_{12}$)
formula	$C_{29}H_{54}F_3FeN_2O_{12}P_3S$	$C_{26}H_{32}F_6N_4O_3P_2Ru$	$C_{23}H_{43}F_6N_9OP_4Fe$	$C_{44}H_{56}BN_7OP_2Fe$
fw	860.56	725.57	755.39	827.56
T (K)	296(2)	172(2)	296(2)	285 (2)
cryst syst	triclinic	monoclinic	orthorhombic	monoclinic
space group	$P\bar{1}$	Pc	$P2_12_12_1$	$P2_1/n$
a (Å)	10.8432(3)	11.9618(9)	10.6307(2)	14.9081(6)
b (Å)	13.7150(4)	9.7039(7)	15.3639(3)	16.0284(7)
c (Å)	14.8964(4)	26.0234(18)	18.6298(3)	17.7016(8)
α (deg)	97.1370(10)			
β (deg)	102.1190(10)	97.919(3)		100.141(2)
γ (deg)	97.8140(10)			
V (Å^3), Z	2118.97(10), 2	2991.9(4), 4	3042.61(10), 4	4163.8(3), 4
μ (mm^{-1})	0.585	0.704	0.781	0.483
λ (Å)	0.71073	0.71073	0.71073	0.71073
ρ_{calc} (g cm^{-3})	1.349	1.611	1.649	1.320
cryst size (mm)	0.3 × 0.2 × 0.1	0.40 × 0.33 × 0.16	0.3 × 0.3 × 0.3	0.4 × 0.3 × 0.2
θ range (deg)	1.91−27.84	3.58−27.26	3.80−36.76	1.73−28.77
total no. of reflns	25 710	35 792	56 943	20 766
no. of indep reflns	9963 [R(int) = 0.0262]	11 141 [R(int) = 0.0491]	15 121 [R(int) = 0.0274]	9819 [R(int) = 0.0242]
no. of param	483	777	398	506
final R indices [$I > 3\sigma(I)$][a]	R1 = 0.0604, wR2 = 0.1631	R1 = 0.0446, wR2 = 0.1097	R1 = 0.0435, wR2 = 0.1219	R1 = 0.0420, wR2 = 0.1042
R indices (all data)[a]	R1 = 0.0959, wR2 = 0.1929	R1 = 0.0527, wR2 = 0.11555	R1 = 0.0567, wR2 = 0.1312	R1 = 0.0748, wR2 = 0.1247
GOF on F^2	1.022	1.038	1.035	1.036
Flack parameter		0.03(3)	0.003(10)	
abs corrn	multiscan	multiscan	multiscan	multiscan

[a] $R1 = \sum||F_o| - |F_c||/\sum|F_o|$; $wR2 = \{\sum[w(|F_o^2| - |F_c^2|)^2]/\sum w|F_o^2|^2]\}^{1/2}$.

Reactions of Reduced Hydride Complexes with CO_2. Solutions of the reduced iron and ruthenium hydride complexes were prepared under vacuum by the reduction of 0.1 to 0.5 mM complex with (excess) sodium amalgam (Na−Hg, 0.5% Na in Hg) in CH_3CN in sealed glassware equipped with an optical cell. Following spectral characterization, the side arm containing Na−Hg was sealed off with a torch, and the solutions were exposed to 1 atm of CO_2 and further characterized. Finally, the seal on the flask was fractured and a small sample of the solution was withdrawn into a microliter syringe for assay by ESI-MS. With Ru(bpy)(P(OEt)$_3$)$_3$(H)$^+$, the MS spectrum measured (parent peak m/z 756.9) was the same as that for a freshly prepared solution of the complex. For Ru(bpy)$_2$(P(OEt)$_3$)(H)$^+$, peaks at m/z 765.8 [Ru(bpy)$_2$(P(OEt)$_3$)(HCO_2)(PF_6)$^+$], 624.9 [(Ru(bpy)$_2$(P(OEt)$_3$)(HCO_2)$^+$], and 310.5 [[Ru(bpy)$_2$(P(OEt)$_3$)-(HCO_2) − 2H]$^{2+}$] confirm production of a formate complex. With Fe(bpy)(P(OEt)$_3$)$_3$(H)$^+$, only a small parent peak, m/z 310.9 [Fe(bpy)(P(OEt)$_3$)$_3$(H)$^+$], and multiple decomposition peaks were observed: m/z 585.5 [Fe(bpy)(P(OEt)$_3$)$_2$(CH_3-CN)$^+$], 544.9 [Fe(bpy)(P(OEt)$_3$)$_2^+$], 377.1 [Fe(bpy)(P(OEt)$_3$)$_1^+$], 983.2 [([Fe(bpy)(P(OEt)$_3$)]$_2$(PF_6)(CH_3CN)$_2$)$^+$].

Reaction of Ru(H)(bpy)$_2$(P(OEt)$_3$)$^+$ with CO_2 in MeOH. A red MeOH solution of Ru(bpy)$_2$(P(OEt)$_3$)(H)(PF_6) (1.93×10^{-4} M), prepared under Ar, was transferred into a quartz UV−vis cell under Ar, and CO_2 was bubbled into the solution for 2 min at ambient temperature. The cell was set up in a thermostatted cell holder regulated at 25 °C under CO_2, and the UV−vis spectra were recorded every 300 s with air as the blank. The color of the solution changed from red to yellow. The formation of Ru(bpy)$_2$(P(OEt)$_3$)(OCHO)(PF_6) was confirmed by ESI-MS, with m/z 625.0 assigned as the formato complex.

Reaction of Ru(bpy)$_2$(P(OEt)$_3$)(H)$^+$ with CO_2 in Water. Ru(bpy)$_2$(P(OEt)$_3$)(H)(PF_6) is only slightly soluble in water, so a pink, saturated aqueous solution was prepared at 25 °C under Ar to test its reactivity toward CO_2. After transfer to a quartz UV−vis cell under Ar, CO_2 was bubbled into the solution for 2 min at ambient temperature. The UV−vis cell was set up in a thermostatted cell holder regulated at 25 °C under CO_2, and UV−vis spectra were recorded every 100 s with air as the blank. However, the only product detected by ESI-MS was hydrated complex Ru(H_2O)(bpy)$_2$(P(OEt)$_3$)$^+$.

Collection and Reduction of X-ray Data. Crystals were mounted on the ends of glass fibers and transferred to a Bruker Kappa Apex II diffractometer for collection of the diffraction data. The diffraction data for [Fe(bpy)(P(OEt)$_3$)$_3$(H)](CF_3SO_3) indicated triclinic symmetry. The diffraction data for (**4**PF_6) indicated monoclinic symmetry and systematic absences consistent with space groups $P2/c$ and Pc. Space group Pc was selected based on statistics and used for the solution and refinement of the structure. The diffraction data for CpFe-(PTA)$_3$(PF_6)$\cdot H_2O$ indicated orthorhombic symmetry and systematic absences consistent with space group $P2_12_12_1$; for CpFe(PTA)$_2$$NCCH_3$(B($C_6H_5$)$_4$)$\cdot HOCH_3$, monoclinic symmetry and systematic absences were consistent with space group $P2_1/n$. Crystal data and information about the data collection are provided in Table 1 and the Supporting Information.

Determination and Refinement of the Structure. The structures of salts of **8**$PF_6\cdot H_2O$, **9**B(Ph)$_4\cdot HOCH_3$, and **4**PF_6 were solved[32] by direct methods, while **1**CF_3SO_3 was solved using Patterson methods. In the least-squares refinement,[32] anisotropic temperature parameters were used for all of the non-hydrogen atoms in **1**CF_3SO_3, **4**PF_6, **8**$PF_6\cdot H_2O$, and **9**B(Ph)$_4\cdot HOCH_3$. In **1**CF_3SO_3 and **4**PF_6, the hydrogen atoms on the disordered ethoxy groups were not included in the refinement, and in **8**$PF_6\cdot H_2O$, the hydrogen atoms on the water of solvation were not included in the refinement. Hydrogen atoms were placed at calculated positions and allowed to "ride" on the atom to which they were attached. A common isotropic thermal parameter was refined for the hydrogen atoms in each structure except for **1**CF_3SO_3 and **4**PF_6. In **1**CF_3SO_3, the positional parameters for the hydrogen atom bonded to the iron were refined. In **4**PF_6, the

(32) Sheldrick, G. M. *SHELXL*, version 5; Siemens Analytical Instruments, Inc.: Madison, WI, 1994.

hydrogen bonded to the ruthenium was located on a difference Fourier map and was included in the final cycles of refinement with its positional coordinates fixed. In $\mathbf{1}CF_3SO_3$ and $\mathbf{4}PF_6$, a common isotropic thermal parameter was refined for the methylene and methyl hydrogen atoms of $P(OEt_3)$ and another common isotropic thermal parameter was refined for the hydrogen atoms on the bpy ligand and the hydride bonded to the ruthenium atom. The data were corrected using the multiscan method (*SADABS*).[33]

Solution of the structure of $\mathbf{4}PF_6$ indicated that there are two formula units of $[Ru(bpy)_2(P(OEt)_3)H]PF_6$ in the asymmetric unit.

Results

Structures of Hydride Complexes with bpy and Phosphite Ligands. The structure of **1**, a distorted octahedral coordination sphere containing bidentate bpy, three triethyl phosphite groups, and a hydride ligand, is shown in Figure 1. As proposed on the basis of NMR work, it is the *mer* isomer in which the hydride ligand is trans to a bpy nitrogen atom.[20,21]

Figure 2 depicts the cation **4** along with the number scheme used. In $Ru(bpy)_2(P(OEt)_3)H]^+$, the ruthenium(II) ion is bonded to two bpy ligands, one $P(OEt)_3$ ligand, and a hydride ion. The two bpy ligands are cis to one another.

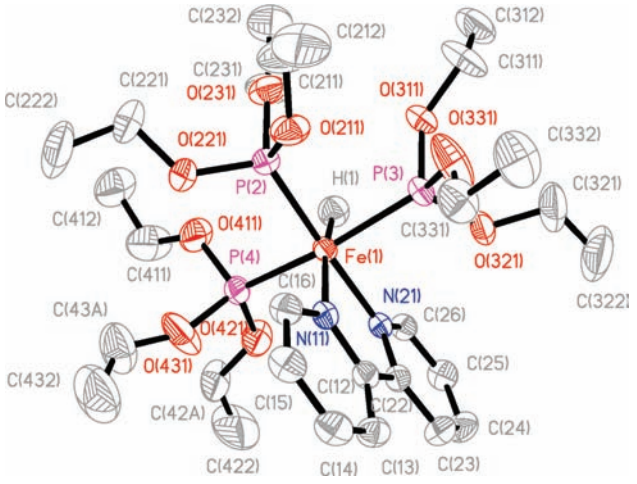

Figure 1. ORTEP plot of **1**.

The asymmetry unit consists of two $[Ru(bpy)_2(P(OEt)_3)H]PF_6$ units, which interact with one another through a π-stacking interaction of two bpy ligands. The two bpy ligands are within 1.6° of being parallel with each other with an average distance between planes of 3.46 Å. An ORTEP drawing of the π-stacked cations is presented in Figure 3. The two cations in the asymmetric unit are stereoisomers.

Metal−ligand distances for $M(bpy)(P(OEt)_3)_3H^+$ with M = Ru[20] (values in italics) and M = Fe (present results) are compared at the left of Chart 3. The average distances for $Ru(bpy)_2(P(OEt)_3)H^+$ are given at the right-hand side of the chart. The average $M^{II}-N$ distances in $Fe(bpy)_3^{2+}$ and $Ru(bpy)_3^{2+}$ are 1.976(12)[34] 2.06 Å,[35,36] respectively. The M−P distance in $M(bpy)(P(OEt)_3)_3H^+$ is ~0.1 Å. shorter for iron than for ruthenium. The M−P distances for iron[37] and ruthenium[38−40] lie in the range reported for other complexes of the same metal.

For both iron and ruthenium complexes, the M−N bond trans to the hydride is longer than that trans to phosphite by ~0.03 Å. The O−C−P cone angles average 128° for **1** and 124° for **4**, both significantly greater than

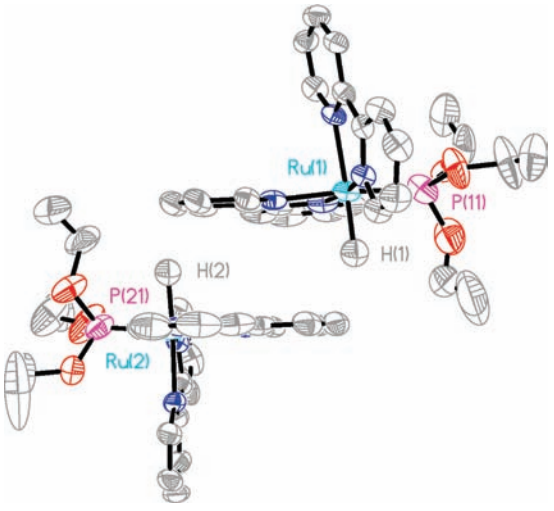

Figure 3. π stacking of $Ru(bpy)_2(P(OEt)_3)H^+$ in the asymmetric unit.

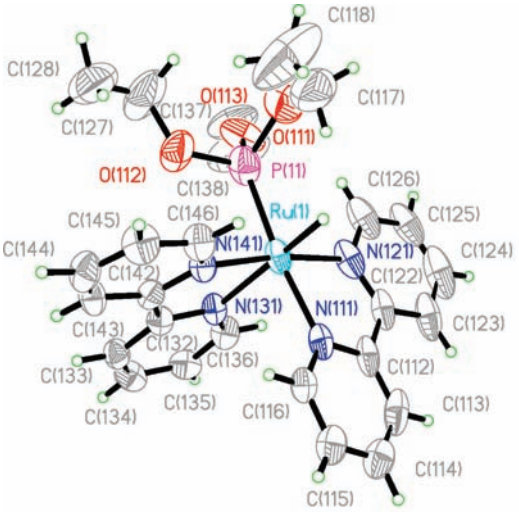

Figure 2. Two stereoisomers of $Ru(bpy)_2(P(OEt)_3)H^+$ in each unit cell.

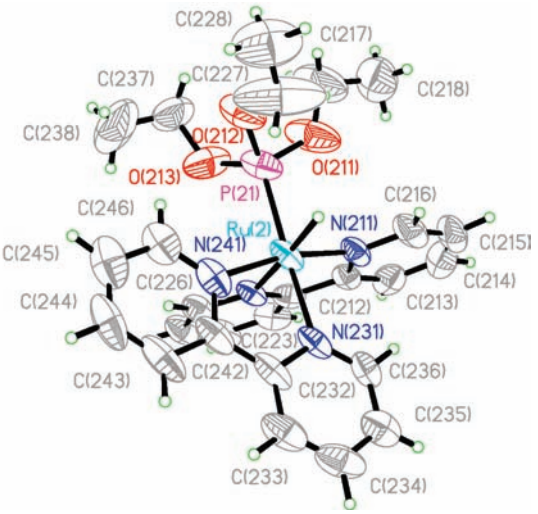

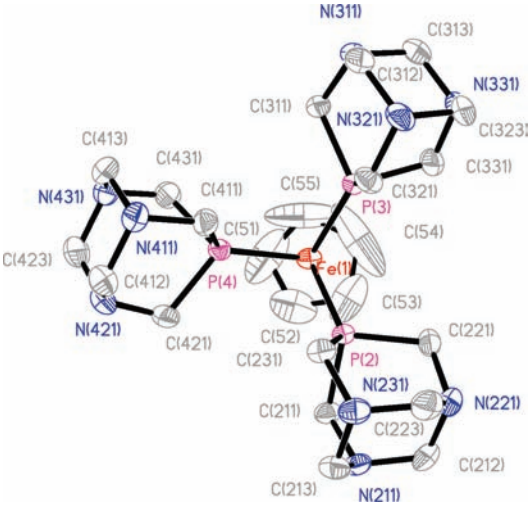

Figure 4. ORTEP plot of the cation **8** in $[CpFe(PTA)_3](PF_6)\cdot H_2O$.

Chart 3. Ru−L (red) and Fe−L (blue) Bond Distances

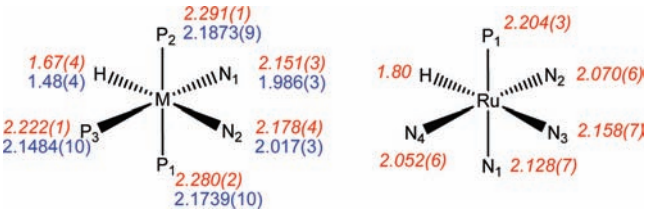

the original Tolman value,[41] as has been noted in other complexes.[42] More extensive comparisons of the distances and angles are given in the Supporting Information.

Structures of PTA Complexes. An ORTEP drawing of the cation $CpFe(PTA)_3^+$ (**8**), which consists of an iron(II) coordinated to a cyclopentadienyl ligand and three PTA ligands, is presented in Figure 4. Figure 5 is an ORTEP of the cation $CpFe(PTA)_2(NCCH_3)^+$ (**9**), in which iron(II) is coordinated to a cyclopentadienide ligand, two PTA ligands, and an acetonitrile ligand. In **8**, the Fe−P bond lengths are almost identical, ranging from 2.1900(5) to 2.2013(5) Å, while in **9**, they are 2.1877(7) and 2.2099(6) Å. The Fe−N distance for the coordinated acetonitrile ligand is much shorter, 1.9099(19) Å. The angles between the centroid of the cyclopentadienyl ligand (X) and the other ligands coordinated to the iron in **8** are X−Fe−P(2) 120.1(1)°, X−Fe−P(3) 123.1(1)°, and X−Fe−P(4) 120.5(1)°, while in **9**, they are X−Fe−P(2) 124.1(1)°,

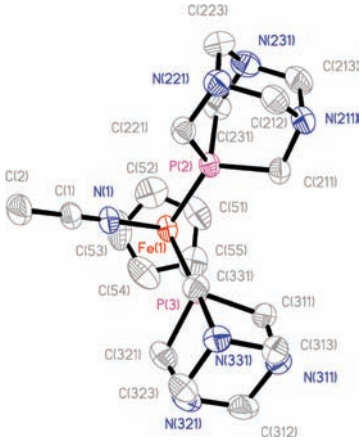

Figure 5. ORTEP plot of the cation **9** in $[CpFe(PTA)_2(NCCH_3)](B(C_6H_5)_4)\cdot HOCH_3$.

X−Fe−P(3) 123.1(1)°, and X−Fe−N(1) 122.8(1)°, respectively. The geometry of the coordination sphere in both compounds is the three-legged piano stool, with the acetonitrile ligand in **9** replacing one of the PTA ligands in **8**. The acetonitrile−Fe−P bond angles in **9** have decreased when compared with the P−Fe−P angles in **8**.

In **8**, there is a water of crystallization that is hydrogen-bonded to N(411) and F(3) with an O(1)···N(411) distance of 2.934 Å and an O(1)···F(3) distance of 2.964 Å with a N(411)−O(1)−F(23) angle of 89.4°. (The hydrogen atoms on this water could not be located on a difference Fourier map.) In the **9** lattice, there is MeOH of crystallization, which is hydrogen-bonded to N(211) [O(88)···N(211) is 3.026 Å, H(88)···N(211) is 1.83 Å, and O(88)−H(88)···N(211) is 176.9°]. Full crystallographic results are given in the Supporting Information for complexes **8** and **9**, respectively. In addition, structures of the PTA complexes are compared in Table S1 in the Supporting Information.

Electronic Absorption Spectra. Ruthenium(II) and low-spin iron(II) complexes containing bpy or other diimine ligands normally exhibit metal-to-ligand charge-transfer (MLCT) bands at relatively low energy, intense ligand-centered $\pi-\pi^*$ bands in the UV region, and relatively weak metal-centered (d−d) transitions that are usually masked by the other intense absorptions.[43] Figure 6 compares the bpy-containing complexes of ruthenium (left) and iron (right) determined in this study. The spectrum of $Ru(bpy)_2(P(OEt)_3)H^+$ (see Table 2) may be compared with that of $Ru(bpy)_2(PPh_3)Cl^+$, which has MLCT maxima at 454 and 328 nm with molar absorptivities of 6.2×10^3 and 7.1×10^3 M^{-1} cm^{-1}, respectively, and bpy-centered $\pi-\pi^*$ absorptions at 292 and 231 nm.[26] The spectrum of $Ru(bpy)(P(OEt)_3)_3(H)^+$ exhibits similar absorption features but with greatly reduced intensity. It may be compared with that of *cis*-$[RuCl_2(dcype)(bpy)]$ (dcype = $PCy_2(CH_2)_4PCy_2$):[44] λ/nm (ε/M^{-1} cm^{-1}) 298 (2.2×10^4), 354 (4.1×10^3), 492 (3.6×10^3), and 592sh (1.6×10^3) in CH_2Cl_2. The same absorption features can be seen in the monobipyridineiron spectra (the high-energy tail is due to iodide). The intense absorption features at 375

(33) Sheldrick, G. M. *SADABS*, version 2007/2; Bruker AXS Inc.: Madison, WI, 2007.
(34) Heilmann, J.; Lerner, H. W.; Bolte, M. *Acta Crystallogr., Sect. E.: Struct. Rep. Online* **2006**, *62*, M1477–M1478.
(35) Biner, M.; Burgi, H. B.; Ludi, A.; Rohr, C. *J. Am. Chem. Soc.* **1992**, *114*, 5197–5203.
(36) Sakai, K.; Uchida, Y.; Kajiwara, T.; Ito, T. *Acta Crystallogr., Sect. C* **2004**, *60*, M65–M68.
(37) Albertin, G.; Antoniutti, S.; Lanfranchi, M.; Pelizzi, G.; Bordignon, E. *Inorg. Chem.* **1986**, *25*, 950–957.
(38) Mazzetto, S. E.; Gambardella, M. T. D.; Santos, R. H. A.; Lopes, L. G. D.; Franco, D. W. *Polyhedron* **1999**, *18*, 979–983.
(39) Albertin, G.; Antoniutti, S.; Bedin, M.; Castro, J.; Garcia-Fontan, S. *Inorg. Chem.* **2006**, *45*, 3816–3825.
(40) Dixon, I. M.; Lebon, E.; Loustau, G.; Sutra, P.; Vendier, L.; Igau, A.; Juris, A. *Dalton Trans.* **2008**, 5627–5635.
(41) Tolman, C. A. *Chem. Rev.* **1977**, *77*, 313–348.
(42) Smith, J. M.; Coville, N. J.; Cook, L. M.; Boeyens, J. C. A. *Organometallics* **2000**, *19*, 5273–5280.
(43) Palmer, R. A.; Piper, T. S. *Inorg. Chem.* **1966**, *5*, 864–878.
(44) de Araujo, M. P.; de Figueiredo, A. T.; Bogado, A. L.; Von Poelhsitz, G.; Ellena, J.; Castellano, E. E.; Donnici, C. L.; Comasseto, J. V.; Batista, A. A. *Organometallics* **2005**, *24*, 6159–6168.

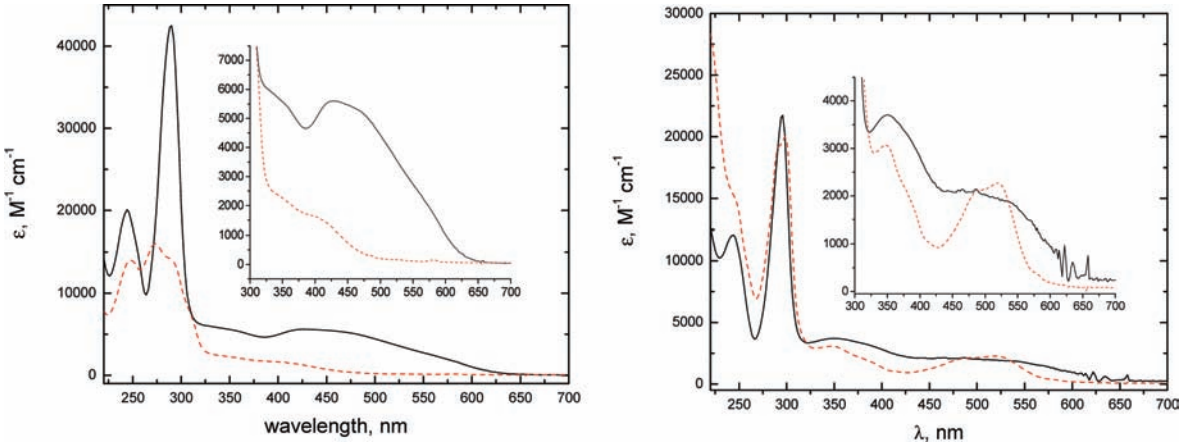

Figure 6. Electronic absorption spectra of (left) $[Ru(bpy)_2(P(OEt)_3)(H)]PF_6$ (solid curve) and $[Ru(bpy)(P(OEt)_3)_3(H)](PF_6)$ (dotted curve) in acetonitrile. Right: $[Fe(bpy)(P(OEt)_3)_3(H)](PF_6)$ (solid curve, spikes between 600 and 700 nm due to noise in the baseline) in acetonitrile and [CpFe(bpy)(CO)]I (dotted curve) in MeOH, respectively.

Table 2. Electronic Absorption Spectra of the Complexes

I[a]	compound	solvent	λ_{max}, nm (ε, M^{-1} cm^{-1})
1	$[Fe(bpy)(P(OEt)_3)_3(H)](PF_6)$	CH_3CN	246 (1.22×10^4), 298 (2.11×10^4), 356 (3.8×10^3), 520 (1.8×10^3)
2	$[Fe(bpy)(P(OEt)_3)_3(CH_3CN)](CF_3SO_3)_2$	CH_3CN	290, 400
3	$[Ru(bpy)(P(OEt)_3)_3(H)](PF_6)$	CH_3CN	247 (1.37×10^4), 272 (1.56×10^4), 290sh, ~350 (2.2×10^3), ~413 (1.4×10^3)
4	$[Ru(bpy)_2(P(OEt)_3)H]PF_6$	CH_3CN	244 (1.95×10^4), 290 (4.26×10^4), ~350 (5.7×10^3), 435 (5.6×10^3)
5	$[Fe(Ph_2PCH_2CH=N(C_6H_4)N=CH CH_2PPh_2)(CH_3CN)_2](BPh_4)_2$	CH_3CN	259sh (5.0×10^4), 375 (5.7×10^3)
7	[CpFe(bpy)(CO)]I	MeOH	220 (3.12×10^4), 290 (1.94×10^4), 350 (3.14×10^3), 382 (2.18×10^3), 488 (2.02×10^3), 520 (2.14×10^3)
9	$[CpFe(PTA)_2(CH_3CN)](PF_6)$	CH_3CN	218 (4.49×10^4), 360 (311), 440 (984), 510sh (344)

[a] Complex identifier (see Chart 1).

and 259 nm in the spectrum of the PNNP complex are likely due to MLCT and $\pi-\pi^*$ transitions, as well. The spectrum of $CpFe(PTA)_2(CH_3CN)^+$ resembles that of ferrocene except that the ligand-field transitions at 360 nm and above are 5−6 times more intense.[45,46] This intensity enhancement is attributed to intensity borrowing from charge-transfer transitions to the antibonding metal d orbitals.[47]

Spectra of the reduced complexes obtained by treatment with sodium amalgam are given in Figure 7. The values of the molar absorptivities for the reduced iron complexes in the visible region are less than 10^3 M^{-1} cm^{-1}, while those for the reduced ruthenium complexes are $\geq 10^4$ M^{-1} cm^{-1}. Furthermore, the features near 390, 500, and 800 nm are characteristic of the $bpy^{\bullet-}$ chromophore.[48−52] A comparison of these spectra suggests that the site of reduction is the metal for M = Fe but the bpy ligand for M = Ru.

Electrochemistry. The results of CV studies of the complexes are summarized in Table 3. Primary data are given in the Supporting Information and in the figures below. Unless otherwise noted, data were obtained with scan rate 100 mV s^{-1}.

Detailed comparisons of the electrochemical data with those for other complexes are given in the Supporting Information.

The CV behavior of the three bpy-containing hydride complexes are compared in Figure 8.

$Ru(bpy)_2(P(OEt)_3)(H)^+$ exhibits the classic signature of a bis(bipyridine) complex with a pair of reversible, one-electron-reduction peaks at −1.43 and −1.69 V vs AgCl/Ag. In the anodic portion of the scan, the metal center is oxidized irreversibly at +0.5 V. The ensuing oxidation at +1.65 V vs AgCl/Ag is due to the acetonitrile complex resulting from decomposition of the oxidized hydride complex. $Ru(bpy)(P(OEt)_3)_3H^+$ exhibits one reversible, one-electron-reduction bpy at −1.6 V vs AgCl/Ag. The irreversible metal-centered oxidation of the hydride complex occurs at +0.9 V vs AgCl/Ag. In contrast, for $Fe(bpy)(P(OEt)_3)_3H^+$, the reduction at −1.7 V is a more complex process with a 0.2 V peak separation, possibly a *two-electron* process. Such behavior has been observed in other systems, is consistent with rapid ligand loss from a reduced species, and is discussed later. The electrochemical experiments cannot directly distinguish between the two possible reduction products, $Fe^I(bpy^{\bullet-})$ and $Fe^0(bpy)$, but this is discussed later as well. $Fe(bpy)(P(OEt)_3)_3H^+$ undergoes metal-centered oxidation at +0.45 V with a surprising degree of reversibility; this oxidation process is logically described as oxidation of the iron(II) hydride to

(45) Sohn, Y. S.; Hendrickson, D. N.; Gray, H. B. *J. Am. Chem. Soc.* **1971**, *93*, 3603–3612.
(46) Vogler, A.; Kunkely, H. *Coord. Chem. Rev.* **2001**, *211*, 223–233.
(47) Fenske, R. F. *J. Am. Chem. Soc.* **1967**, *89*, 252–256.
(48) Heath, G. A.; Yellowlees, L. J.; Braterman, P. S. *J. Chem. Soc., Chem. Commun.* **1981**, 287–289.
(49) Heath, G. A.; Yellowlees, L. J.; Braterman, P. S. *Chem. Phys. Lett.* **1982**, *92*, 646–648.
(50) Creutz, C. *Comments Inorg. Chem.* **1982**, *1*, 293–311.
(51) Braterman, P. S.; Song, J. I. *J. Org. Chem.* **1991**, *56*, 4678–4682.
(52) Braterman, P. S.; Song, J. I.; Peacock, R. D. *Inorg. Chem.* **1992**, *31*, 555–559.

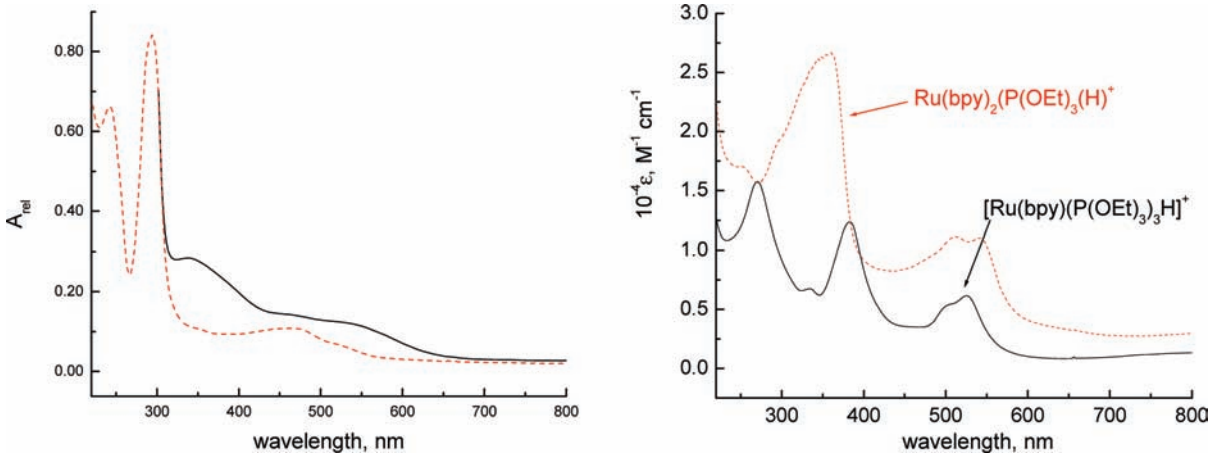

Figure 7. Spectra of reduced solutions in acetonitrile under vacuum. The reductant was sodium amalgam: (left) starting with $Fe(bpy)(P(OEt)_3)_3H^+$ (ca. 0.3 mM, black, solid line) and $Fe(bpy)(P(OEt)_3)_3(CH_3CN)^{2+}$ (red, dashed line); (right) starting with $Ru(bpy)(P(OEt)_3)_3H^+$ (black, solid line) and $Ru(bpy)_2(P(OEt)_3)H^+$ (red, dashed line).

Table 3. Electrochemical Results for an Acetonitrile Solvent Containing 0.1 M TBAH at 22 °C[a]

I	compound	E_{pa}, V	E_{pc}, V	E_{av}, V vs NHE
1	$[Fe(bpy)(P(OEt)_3)_3H](PF_6)$	−1.48, −1.65[b] +0.45, +0.43,[c] +1.46	−1.69 (n = 2), +0.38 +1.33	(−1.39), +0.62
2	$[Fe(bpy)(P(OEt)_3)_3(CH_3CN)](CF_3SO_3)_2$	−0.93 (n = 2), +1.48	−1.15, +1.38	+1.63
3	$[Ru(bpy)(P(OEt)_3)_3H](PF_6)$	−1.64, +0.95	−1.57, +0.87	−1.41, +1.10
4	$[Ru(bpy)_2(P(OEt)_3)H](PF_6)$	−1.73, −1.49, +0.55 irr	−1.80, −1.55	−1.57, −1.32, (+0.75) irr
10	$[Ru(bpy)_2(P(OEt)_3)(CH_3CN)](PF_6)_2$	+1.69	+1.62	+1.86
5	$[FeL_1(CH_3CN)_2][BPh_4]_2$, $L_1 = Ph_2PCH_2CH{=}N(C_6H_4)N = CHCH_2PPh_2$	+0.87 irr,[d] +1.49 irr		
6	$[FeL_2(CH_3CN)_2][BPh_4]_2$, $L_2 = Ph_2PCH_2CH{=}NC_2H_4N = CHCH_2PPh_2$	+0.81 irr,[d] +1.45	−1.36 irr, +1.35	+1.60
6	$[FeL_2(CH_3CN)_2][BF_4]_2$, $L_2 = Ph_2PCH_2CH{=}NC_2H_4N{=}CHCH_2PPh_2$	+0.27,[e] +1.01, +1.40	+0.20,[e] +0.94, +1.32	+1.56
7	[CpFe(bpy)(CO)]I	−1.37 irr	+1.21 irr	(−1.2), (+1.4)
9	$[CpFe(PTA)_2(CH_3CN)](PF_6)_2$	+0.74	+0.68	+0.91

[a] Potentials vs AgCl/Ag (= +0.20 V vs NHE), n = 1, unless otherwise noted. "irr" denotes irreversibility. Values given in parentheses are rough estimates because the process is irreversible. I is the complex identifier (see Chart 1). [b] OSW cathodic voltammetry. [c] OSW anodic voltammetry. [d] Due to oxidation of the counterion BPh_4^-. [e] Decomposition product.

the corresponding iron(III) hydride, i.e.,

$$Fe(bpy)(P(OEt)_3)_3(H)^+ - e^- = Fe(bpy)(P(OEt)_3)_3(H)^{2+}$$

and such reversibility has been seen previously for hydride complexes of iron.[53−55] Oxidized metal hydrides are strong acids and may protonate the parent complex.[56] Hydride oxidation can be complex and may depend on the concentration of the parent complex and added bases.[57,58] Here the process is diffusion-limited, as confirmed by plots if i_{pc} and i_{pa} versus the square root of the sweep rate up to a sweep rate of ∼2 V s^{-1} (Supporting Information). Relatively slow decomposition of the iron(III) hydride complex yields the acetonitrile complex $Fe(bpy)(P(OEt)_3)_3(CH_3CN)^{2+}$, which is oxidized at even higher potential. This hypothesis was confirmed by comparing the voltammograms of the acetonitrile and hydride complexes (Figure 8).

For the BPh_4^- salts of PNNP complexes **5** and **6**, irreversible oxidation[59,60] of the BPh_4^- anion at ∼+0.85 V complicates the voltammetry. The $Fe^{II}-Fe^{III}$ metal-centered oxidation occurs at ∼+1.48 and ∼+1.38 V vs AgCl/Ag for **5** and **6**, respectively. (Other oxidation peaks for **6** are attributed to impurities in the BF_4^- salt.); **6** undergoes reduction at −1.36 V vs AgCl/Ag. With [CpFe(bpy)(CO)]I, the first reduction peak is at −1.37 V and the oxidation peak is at +1.21 mV. Numerous other peaks are also seen: reduction, −1.59 V; oxidation, +0.57, +0.82, and +1.80 V vs AgCl/Ag. Their presence is puzzling in light of the high purity indicated by the NMR spectrum. $CpFe(PTA)_2(CH_3CN)(PF_6)$ exhibits a metal-centered oxidation at +0.71 V vs AgCl/Ag.

(53) Tilset, M.; Fjeldahl, I.; Hamon, J.-R.; Hamon, P.; Toupet, L.; Saillard, J.-Y.; Costuas, K.; Haynes, A. *J. Am. Chem. Soc.* **2001**, *123*, 9984–10000.
(54) Bianchini, C.; Peruzzini, M.; Ceccanti, A.; Laschi, F.; Zanello, P. *Inorg. Chim. Acta* **1997**, *259*, 61–70.
(55) Burrows, A. D.; Harrington, R. W.; Kirk, A. S.; Mahon, M. F.; Marken, F.; Warren, J. E.; Whittlesey, M. K. *Inorg. Chem.* **2009**, *48*, 9924–9935.
(56) Smith, K. T.; Romming, C.; Tilset, M. *J. Am. Chem. Soc.* **1993**, *115*, 8681–8689.
(57) Romming, C.; Smith, K. T.; Tilset, M. *Inorg. Chim. Acta* **1997**, *259*, 281–290.
(58) Quadrelli, E. A.; Kraatz, H. B.; Poli, R. *Inorg. Chem.* **1996**, *35*, 5154–5162.
(59) Geske, D. H. *J. Phys. Chem.* **1959**, *63*, 1062–1070.
(60) Pal, P. K.; Chowdhury, S.; Drew, M. G. B.; Datta, D. *New J. Chem.* **2002**, *26*, 367–371.

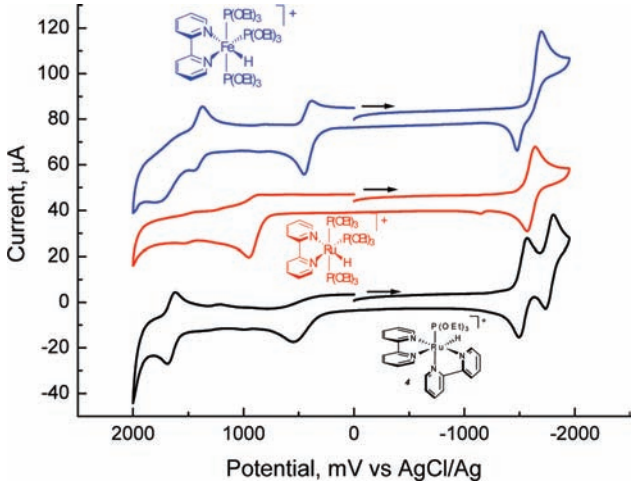

Figure 8. CV of 0.58 mM [Fe(bpy)(P(OEt)$_3$)$_3$(H)](CF$_3$SO$_3$) (blue), 0.87 mM [Ru(bpy)(P(OEt)$_3$)$_3$(H)](PF$_6$) (red), and 1.0 mM [Ru(bpy)$_2$(P(OEt)$_3$)(H)](PF$_6$) (black line) under N_2 in CH_3CN [Bu_4NPF_6, 0.1 M; CH_3CN; scan rate, 100 mV s^{-1}; reference electrode, AgCl/Ag (3 M aqueous KCl); counter electrode, platinum wire; working electrode, glassy carbon (d = 3 mm)].

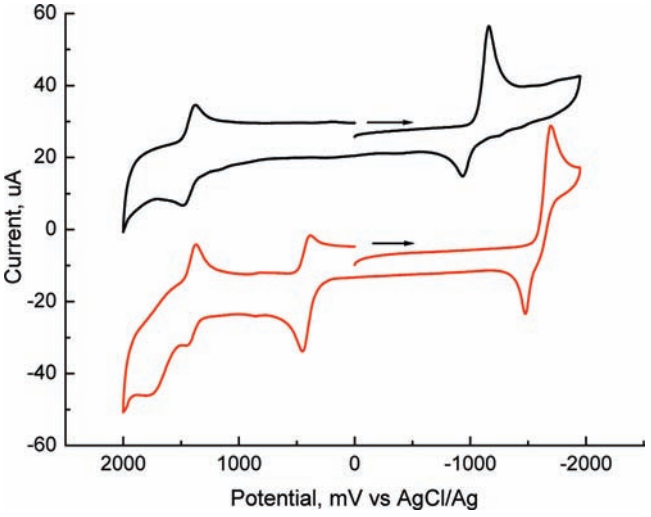

Figure 9. Cyclic voltammograms of 0.58 mM [Fe(bpy)(P(OEt)$_3$)$_3$(CH$_3$CN)](CF$_3$SO$_3$)$_2$ (black line) and 0.58 mM [Fe(bpy)(P(OEt)$_3$)$_3$(H)](CF$_3$SO$_3$) (red line) in CH_3CN under N_2 [Bu_4NPF_6, 0.1 M; CH_3CN; scan rate, 100 mV s^{-1}; reference electrode, AgCl/Ag (3 M aqueous KCl); counter electrode, platinum wire; working electrode, glassy carbon (d = 3 mm)].

Electrochemical Behavior of the Iron Phosphite Complexes. Cyclic voltammograms of Fe(bpy)(P(OEt)$_3$)$_3$H$^+$ and Fe(bpy)(P(OEt)$_3$)$_3$(CH$_3$CN)$^{2+}$ are compared in Figure 9. The reduction process for the acetonitrile complex has a large peak separation like the hydride complex, but it occurs at considerably more positive potential. We next describe details and their possible interpretation.[23,61−63]

For both Fe(bpy)(P(OEt)$_3$)$_3$H$^+$ and Fe(bpy)(P(OEt)$_3$)$_3$(CH$_3$CN)$^{2+}$, the currents are a linear function of the square root of the sweep rate, indicating a diffusive process. For Fe(bpy)(P(OEt)$_3$)$_3$H$^+$, the slopes for cathodic and anodic portions are similar (40 ± 2) and about 2.8 times the slope found for the anodic peak for oxidation of the hydride at ca. +0.4 V. This ratio is predicted if n = 1 for the +0.4 V process and n = 2 for the −1.6 V process. However, the peak positions shift with the logarithm of the sweep rate (ν = 0.05−2.0 V s^{-1}) consistent with electrochemical irreversibility or an EC mechanism. For Fe(bpy)(P(OEt)$_3$)$_3$H$^+$, the slopes are −0.022 and +0.028 V per decade for cathodic and anodic peaks, respectively (0.03/n expected for EC n = 1). The ratio i_{pc}/i_{pa} is <1, rising from 0.67 at ν = 0.05 V s^{-1} to about 0.9 at 2 V s^{-1} for Fe(bpy)(P(OEt)$_3$)$_3$H$^+$, consistent with log(k_f) ~ −1 ± 0.5. The Osteryoung square-wave (OSW) responses for the +0.4 anodic and −1.6 cathodic processes are (except for the sign) identical in current and area.

For Fe(bpy)(P(OEt)$_3$)$_3$(CH$_3$CN)$^{2+}$, the slope of the current versus square root of the sweep rate is about 3 times (70/17) greater for the cathodic −1.1 V peak as for the anodic peak at −0.9 V and 2.8 times greater than that for oxidation of the acetonitrile complex. This ratio is predicted if n = 1 for the +1.4 V process and n = 2 for the cathodic −1.2 V process. The peak positions shift with the logarithm of the sweep rate (ν = 0.05−2.0 V s^{-1}). For Fe(bpy)(P(OEt)$_3$)$_3$(CH$_3$CN)$^{2+}$, the slopes are −0.06 and +0.01 V per decade for cathodic and anodic peaks, respectively (0.03/n expected for n = 1).The ratio i_{pc}/i_{pa} is <1, rising from 0.2 at ν = 0.05 V s^{-1} to about 0.5 at 0.3 V s^{-1} and dropping at higher sweep rates. The OSW responses for −1.13 cathodic processes are ~85% as great as for the +1.43 V process in current and area.

For Fe(bpy)(P(OEt)$_3$)$_3$H$^+$ and Fe(bpy)(P(OEt)$_3$)$_3$(CH$_3$CN)$^{2+}$ complexes, the reduction process is two-electron in nature. There are two possible scenarios leading to the two-electron behavior: (1) $E(Fe^{I/0}) > E(Fe^{II/I})$ (an EE mechanism) and (2) a rapid chemical reaction converts the iron(I) complex to another one for which $E(Fe^{I/0}) > E(Fe^{II/I})$ (an ECE mechanism). On the basis of the work of Pilloni et al. on the reduction of iron(II) hydride complexes, we would anticipate an ECE mechanism for the reduction of Fe^{II}(bpy)(P(OEt)$_3$)$_3$H$^+$ in which the chemical step corresponds to detachment of the pyridyl trans[64] to the hydride ligand, yielding a five-coordinate species Fe(η^1-bpy)(P(OEt)$_3$)$_3$H^0. [Quite analogous behavior has been seen for an isoelectronic manganese(I) system.[65]]

$$Fe^{II}(bpy)(P(OEt)_3)_3H^+ + e^- \rightleftharpoons Fe^{I}(bpy)(P(OEt)_3)_3H^0 \quad E_1^0 \qquad (1)$$

$$Fe^{I}(bpy)(P(OEt)_3)_3H^0 \rightleftharpoons Fe^{I}(\eta^1\text{-bpy})(P(OEt)_3)_3H^0 \quad k_f,\ k_b \qquad (2)$$

$$Fe^{I}(\eta^1\text{-bpy})(P(OEt)_3)_3H^0 + e^- \rightleftharpoons Fe^{0}(\eta^1\text{-bpy})(P(OEt)_3)_3H^- \quad E_2^0 \qquad (3)$$

For the case $E_2^0 > E_1^0$, a cathodic peak will occur at E_1^0, and if the η^2-bpy/η^1-bpy conversion is rapid, then the Fe^{I}

(61) Nicholson, R. S.; Shain, I. *Anal. Chem.* **1965**, *37*, 178–190.
(62) Odea, J. J.; Osteryoung, J.; Osteryoung, R. A. *Anal. Chem.* **1981**, *53*, 695–701.
(63) Zanello, P. *Inorganic Electrochemistry Theory, Practice and Application*; The Royal Society of Chemistry: Cambridge, U.K., 2003.
(64) Pilloni, G.; Zotti, G.; Mulazzani, Q. G.; Fuochi, P. G. *J. Electroanal. Chem.* **1982**, *137*, 89–102.
(65) Kuchynka, D. J.; Kochi, J. K. *Inorg. Chem.* **1988**, *27*, 2574–2581.

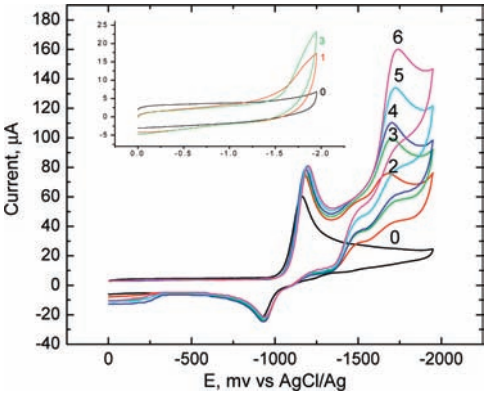

Figure 10. Cyclic voltammograms of 1.00 mM $Fe(bpy)(P(OEt)_3)_3(CH_3CN)(CF_3SO_3)_2$ in different concentrations of CH_3CO_2H in CH_3CN under Ar [Bu_4NPF_6, 0.1 M; CH_3CN; scan rate, 100 mV s^{-1}; reference electrode, AgCl/Ag (3 M aqueous KCl); counter electrode, platinum wire; working electrode, glassy carbon (d = 3 mm)]. The number labels give the acetic acid concentration (mM). The inset shows the current in the absence of the iron complex; the current for the 2 mM CH_3CO_2H blank is ~24 μA, in contrast to ~75 μA with the 1 mM complex.

Scheme 1

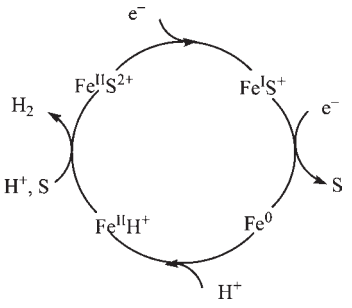

ion will be reduced, as well. The return anodic peak will occur at E_2^0. Assuming from Fuochi's studies[66] that k for ligand dissociation is 10^4 s^{-1}, our observations are consistent with eqs 1−3 as a model. For $Fe(bpy)(P(OEt)_3)_3(CH_3CN)^{2+}$, an ECE mechanism as discussed above (eqs 1−3) appears to apply again, with probable loss of CH_3CN occurring as the C step.

Two-electron reduction of $Fe(bpy)(P(OEt)_3)_3H^+$ and $Fe(bpy)(P(OEt)_3)_3(CH_3CN)^{2+}$ could involve either the $Fe^{II}(bpy)/Fe^{II}(bpy^{\bullet-})$ and $Fe^{II}(bpy^{\bullet-})/Fe^{I}(bpy^{\bullet-})$ couples or the $Fe^{II}(bpy)/Fe^{I}(bpy)$ and $Fe^{I}(bpy)/Fe^{0}(bpy)$ couples. Accordingly, we measured the electronic absorption spectra of the reduced species obtained by a chemical reduction method. On the time scale of minutes, the spectra shown in Figure 7 are obtained and establish that it is the metal, rather than the ligand, that is reduced. Of course, this observation does not rule out the possibility that a bpy ligand reduced species is a transient.

Reactivity Studies

Reaction with Acid. As shown in Figure 10, there is evidence for reaction of the reduced species from $Fe(bpy)(P(OEt)_3)_3(CH_3CN)^{2+}$ (probably $Fe(bpy)(P(OEt)_3)_3^0$) with acid. With 2 mM acetic acid, the current at the new cathodic peak at −1.7 V vs AgCl/Ag is about 3 times greater than that in the absence of $Fe(bpy)(P(OEt)_3)_3(CH_3CN)^{2+}$. The position of this peak corresponds to that of $Fe(bpy)(P(OEt)_3)_3(H)^+$, which undergoes protonation in CH_2Cl_2 at low temperature to yield an η^2-dihydrogen complex.[21] Above −20 °C, free H_2 was found.[21] The cathodic peak current is linear in an acid concentration up to 6 mM, the highest concentration studied, as shown the Supporting Information, and a plausible scheme for electrocatalysis is given in Scheme 1. Note that Pugh et al. found $Ru(bpy)_2(CO)^0$ to be protonated by 1 mM water in acetonitrile in < 1 ms.[67] This study is incomplete,but is mentioned because of the current intense interest in proton reduction catalysis. The behavior found resembles that of some of the biomimics of iron hydrogenase.[68−71] The electrochemical reduction of protons to H_2 is frequently studied in acetonitrile, with potentials being referenced to the ferrocene couple.[72] For the case of the weak acid acetic acid (pK_a = 22.3 in CH_3CN), the thermodynamic reduction potential is −1.46 V vs Fc^+/Fc.[72,73] The catalytic wave for acid reduction with $Fe(bpy)(P(OEt)_3)_3(CH_3CN)(CF_3SO_3)_2$ is at −2.01 V vs Fc^+/Fc, and the overvoltage for the reduction is thus 0.55 V.

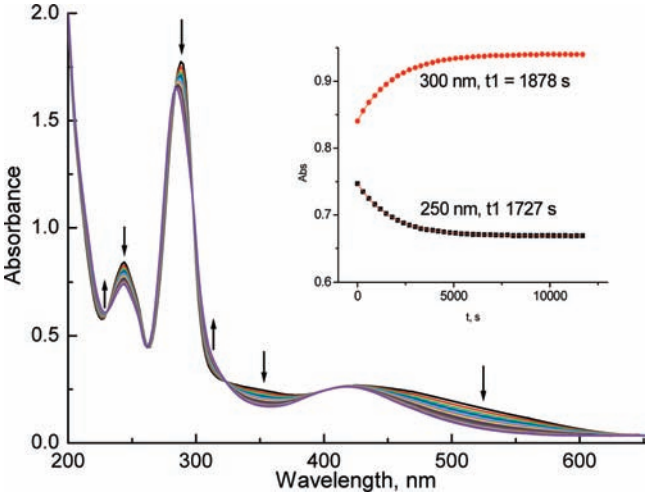

Figure 11. UV−vis spectra of $Ru(bpy)_2(P(OEt)_3)(H)(PF_6)$ in MeOH (concentration: 1.93×10^{-4} M) under 1 atm of CO_2, every 300 s, cell b = 0.4 cm, color, from red to yellow. The inset shows the time dependence and first-order fit of the absorbance changes at 250 (lower trace) and 300 nm.

Reactions with CO_2. $Ru(bpy)_2(P(OEt)_3)H^+$ was reported to react with CO_2 overnight in CH_2Cl_2,[20] and we have found that it reacts with CO_2 in MeOH and in water. Spectral changes followed in MeOH are shown in Figure 11.

Averaging such data over five wavelengths gives t_1 = 1.8×10^3 s and $k_{obs} = 5.5 \times 10^{-4}$ s^{-1}, and dividing by the

(66) Fuochi, P. G.; Mulazzani, Q. G.; Pilloni, G.; Zotti, G. *J. Phys. Chem.* **1980**, *84*, 2985–2989.
(67) Pugh, J. R.; Bruce, M. R. M.; Sullivan, B. P.; Meyer, T. J. *Inorg. Chem.* **1991**, *30*, 86–91.
(68) Mejia-Rodriguez, R.; Chong, D.; Reibenspies, J. H.; Soriaga, M. P.; Darensbourg, M. Y. *J. Am. Chem. Soc.* **2004**, *126*, 12004–12014.
(69) Na, Y.; Wang, M.; Jin, K.; Zhang, R.; Sun, L. *J. Organomet. Chem.* **2006**, *691*, 5045–5051.
(70) Felton, G. A. N.; Mebi, C. A.; Petro, B. J.; Vannucci, A. K.; Evans, D. H.; Glass, R. S.; Lichtenberger, D. L. *J. Organomet. Chem.* **2009**, *694*, 2681–2699.
(71) Capon, J. F.; Gloaguen, F.; Petillon, F. Y.; Schollhammer, P.; Talarmin, J. *Coord. Chem. Rev.* **2009**, *253*, 1476–1494.
(72) Felton, G. A. N.; Glass, R. S.; Lichtenberger, D. L.; Evans, D. H. *Inorg. Chem.* **2006**, *45*, 9181–9184.
(73) Felton, G. A. N.; Glass, R. S.; Lichtenberger, D. L.; Evans, D. H. *Inorg. Chem.* **2007**, *46*, 5126–5126.

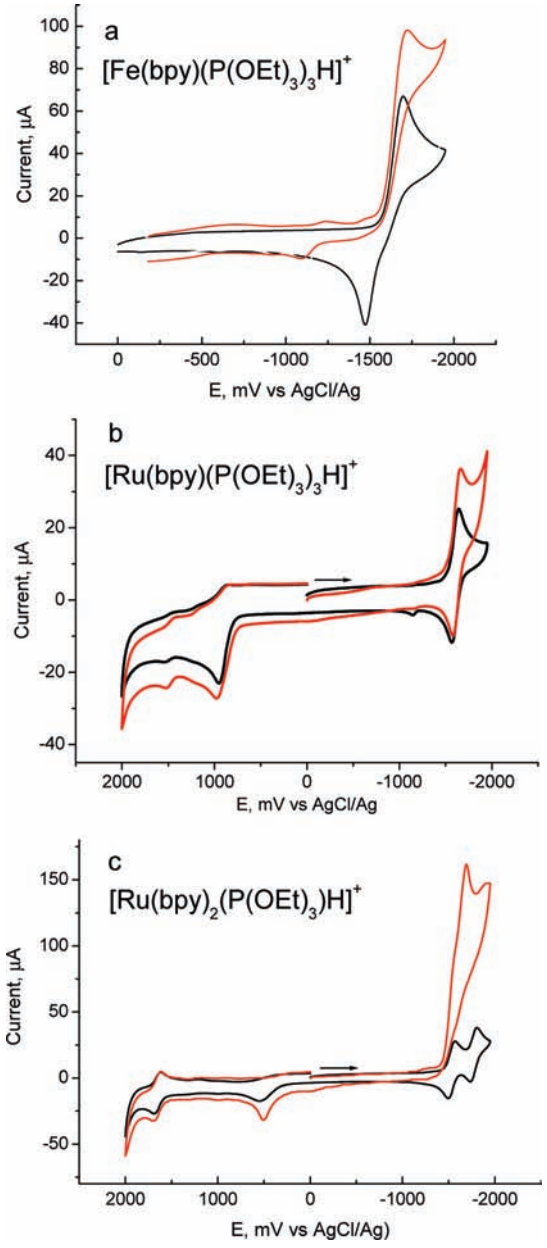

Figure 12. (a) Cyclic voltammograms of 1.0 mM $[Fe(bpy)(P(OEt)_3)_3(H)](CF_3SO_3)$, (b) 0.87 mM $[Ru(bpy)(P(OEt)_3)_3(H)](PF_6)$, and (c) 1.0 mM $[Ru(bpy)_2(P(OEt)_3)(H)](PF_6)$. All in MeCN under N_2 (black) and saturated with CO_2 at 1 atm (red). The scan rate was 100 mV s^{-1}.

CO_2 solubility in MeOH, 0.14 M/atm,[74] we estimate a second-order rate constant of 3.9×10^{-3} M^{-1} s^{-1}. That for $Ru(terpy)(bpy)H^+$ is 1200 times greater.[75] Generation of the formate complex was confirmed by ESI-MS. Reaction also occurred in water (Supporting Information); however, the only product detected by ESI-MS was the aqua complex. It is expected that solvolysis of the formate will be more rapid in water than in MeOH.

Upon reduction, $Ru(bpy)(P(OEt)_3)_3H^+$, $Ru(bpy)((P(OEt)_3))_3H^+$, and $Fe(bpy)(P(OEt)_3)_3H^+$ react with CO_2 in acetonitrile (see Figures 12 and 13). Both electrochemical and chemical reduction studies lead to this conclusion.

(74) Konno, H.; Ishii, Y.; Sakamoto, K.; Ishitani, O. *Polyhedron* **2002**, *21*, 61–68.
(75) Konno, H.; Kobayashi, A.; Sakamoto, K.; Fagalde, F.; Katz, N. E.; Saitoh, H.; Ishitani, O. *Inorg. Chim. Acta* **2000**, *299*, 155–163.

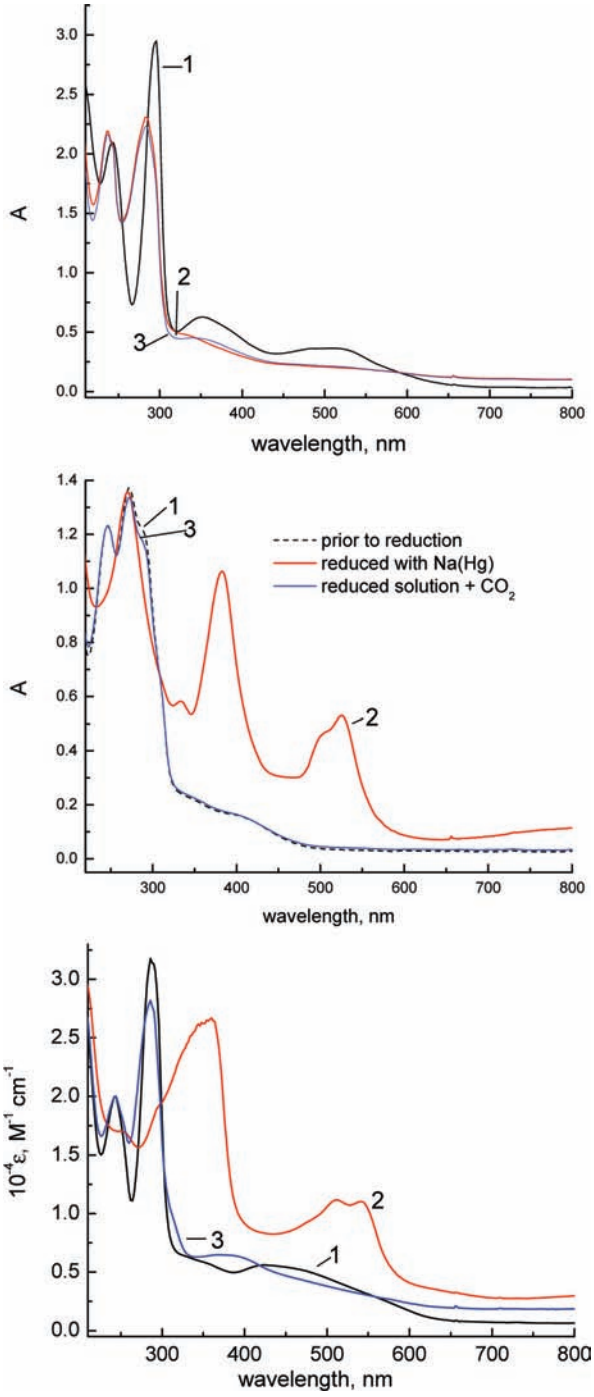

Figure 13. UV−vis absorption spectra of ca. 0.1 mM solutions of (a) $Fe(H)(bpy)(P(OEt)_3)_3(PF_6)$, (b) $[Ru(bpy)(P(OEt)_3)_3(H)](PF_6)$, and (c) $[Ru(bpy)_2(P(OEt)_3)(H)](PF_6)$ in MeCN under vacuum (1, black), reduced with sodium (mercury) (2, red), and saturated with CO_2 at 1 atm (3, blue).

Chemical reduction was achieved with sodium amalgam as the reductant: The reduced ruthenium complexes exhibited characteristic reduced bipyridine anion radical spectra, whereas the reduced iron complexes exhibit the moderately intense ligand-field absorptions associated with the square-pyramidal d^8 configuration. The product of the reaction of the chemically reduced solution with CO_2 was established as formate in the case of $Ru(bpy)_2(P(OEt)_3)(H)^+$ as the starting complex because the formate ion remained bonded to the metal. However, no

Table 4. Tentative Reduction Site and Reactivity[a]

complex	E_{av}, V vs NHE, obsd	assignment	reacts with CO_2?
[CpFe(bpy)(CO)]I	(−1.17)	bpy	
$Fe(bpy)_2(P(OEt)_3)H^+$			NR in CH_2Cl_2[21]
$Fe(bpy)(P(OEt)_3)_3H^+$	−1.39 (n = 2)	Fe	NR in CH_2Cl_2[21] R after $2e^-$ in CH_3CN[b]
$Fe(bpy)_2(P(OEt)_3)(CH_3CN)^{2+}$	−0.82 (n = 2)	Fe	R with CH_3CO_2H after $2e^-$ in CH_3CN[b]
$Ru(bpy)(P(OEt)_3)_3H^+$	−1.37	bpy	NR in CH_2Cl_2[20] R after $1e^-$ in CH_3CN[b]
$Ru(bpy)_2(P(OEt)_3)H^+$	−1.55	bpy	R in CH_2Cl_2[20] R in CH_3OH, H_2O,[b] R after $1e^-$ in CH_3CN[b]

[a] NR = no reaction; R = reaction occurs. [b] Determined in this study.

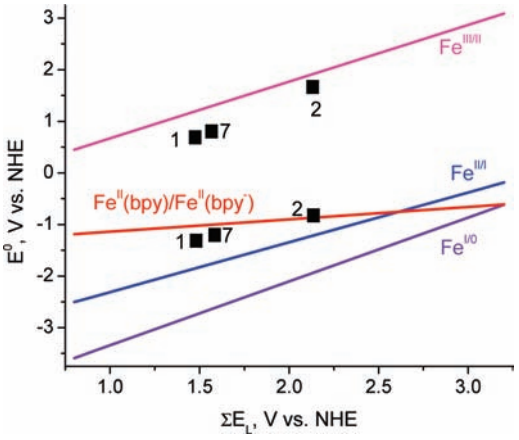

Figure 14. Reduction potential vs sum of the E_L values for iron complexes. See the text for an explanation.

carbon product was detected starting with $Ru(bpy)((P(OEt)_3))_3H^+$ and $Fe(bpy)(P(OEt)_3)_3H^+$. For $Fe(bpy)(P(OEt)_3)_3H^+$, this may be a result of solvolysis of the product. The observation of apparently intact $Ru(bpy)((P(OEt)_3))_3H^+$ is puzzling; conceivably, the CO_2 insertion is reversed under the conditions of the ESI-MS measurement.

Discussion

Table 4 summarizes our observations on the reductive electrochemistry of the bpy-containing complexes studied here and the reactivity of parent and reduced species.

Iron(I) and Iron(0). Like other d^7 complexes,[76,77] iron(I) may be a six-coordinate, 19-electron species or a five-coordinate, 17-electron species.[78] The reduction of iron(II) hydride complexes $Fe(dppe)_2H(L)^+$ either electrochemically[79] or by solvated electrons is accompanied by ligand L loss.[66,80] First-order rate constants for ligand loss range from 10^{-4} [64] to $>10^4$ s^{-1}.[80] In electrochemical experiments, the L loss step is followed by uptake of a second electron.[64] The overall process is thus an ECE mechanism. As noted earlier, we believe this to be the case here as well. For the acetonitrile complex **2**, rapid acetonitrile loss is likely; for the hydride complex, there are several possibilities: loss of phosphite, loss of bpy, or formation of monodentate bpy. Because there is precedent for bidentate/monodentate interconversion in the case[80] of $Fe^I(dppe)_2(P(OMe)_3)H$, we prefer the latter interpretation. Also, it is consistent with the constancy of the potential for iron(III) oxidation; upon oxidation, the bpy becomes again bidentate. The doubly reduced species are d^8 iron(0), likely square pyramidal in structure.

Reactivity of $bpy^{\bullet-}$ Radical Species. The reactivity of $Ru(bpy^{\bullet-})(P(OEt)_3)_3(H)^0$ and $Ru(bpy)(bpy^{\bullet-})(P(OEt)_3)(H)^0$ toward CO_2 is surprising. There is precedent for the reaction of electrochemically reduced bpy complexes with CO_2:[81,82] singly reduced $Ru(bpy)_2(CO)H$ and doubly reduced $Os(bpy)_2(CO)(H)^-$ are implicated as intermediates in the electrocatalytic reduction of CO_2 in DMF with potentials comparable to those used here. However, in general, the reactions are attributed to the formation of a highly reactive reduced metal center.

Factors Determining the Reduction Site. It is of interest to understand and to be able to predict the multielectron redox behavior of a metal complex. Lever's E_L parameter makes this possible when sufficient electrochemical data are already available. For reduction at the metal and ligand,[83] the redox potential is given by eqs 4 and 5, respectively.

$$E_{red} = S_m[\sum E_L(L)] + I_m \quad (4)$$

$$E_{red} = S_L \sum E_L(L) + I_L \quad (5)$$

Figure 14, a plot of E^0 versus the sum of E_L values for the complex, provides an approximate model appropriate to the $Fe(bpy)(P(OEt)_3)_3(H)^+$, $Fe(bpy)(P(OEt)_3)_3(CH_3CN)^{2+}$, and $Fe(Cp)(bpy)(CO)^+$.

Starting at the top of the figure from the left-hand side, the first (magenta) line is a plot of the $Fe^{III/II}$ potential; the second (red) line of much smaller slope is for the $Fe^{II}(bpy)/Fe^{II}(bpy^{\bullet-})$ couple. Below that are the $Fe^{II/I}$ (blue) and $Fe^{I/0}$ (violet) couples. The first two lines, $E^{III/II} = 1.1[\sum E_L(L)] - 0.43$ and $E^{b/b^-} = 0.24\sum E_L(L) - 1.38$, where E^{b/b^-} refers to the $Fe^{II}(bpy)/Fe^{II}(bpy^{\bullet-})$ couple, are the most reliable, being based on large data sets.[22,83] The third and fourth lines, $E^{II/I} = 0.97[\sum E_L(L)] - 3.28$ and $E^{I/0} = 0.97[\sum E_L(L)] - 4.58$, are based on a 12-compound data set for both couples given by Abd-El-Aziz et al. for $(C_6H_sX)(Cp)Fe^+$.[84] Lu et al. have given

(76) Pilloni, G.; Schiavon, G.; Zotti, G.; Zecchin, S. *J. Organomet. Chem.* **1977**, *134*, 305–318.
(77) Kew, G.; Dearmond, K.; Hanck, K. *J. Phys. Chem.* **1974**, *78*, 727–734.
(78) Sullivan, B. P.; Conrad, D.; Meyer, T. J. *Inorg. Chem.* **1985**, *24*, 3640–3645.
(79) Zotti, G.; Zecchin, S.; Pilloni, G. *J. Organomet. Chem.* **1979**, *181*, 375–386.
(80) Fuochi, P. G.; Mulazzani, Q. G.; Pilloni, G.; Zotti, G. *Inorg. Chim. Acta* **1983**, *68*, 195–200.
(81) Bruce, M. R. M.; Megehee, E.; Sullivan, B. P.; Thorp, H.; Otoole, T. R.; Downard, A.; Meyer, T. J. *Organometallics* **1988**, *7*, 238–240.
(82) Bruce, M. R. M.; Megehee, E.; Sullivan, B. P.; Thorp, H. H.; Otoole, T. R.; Downard, A.; Pugh, J. R.; Meyer, T. J. *Inorg. Chem.* **1992**, *31*, 4864–4873.
(83) Dodsworth, E. S.; Vlcek, A. A.; Lever, A. B. P. *Inorg. Chem.* **1994**, *33*, 1045–1049.
(84) Abd-El-Aziz, A. S.; Baranski, A. S.; Piorko, A.; Sutherland, R. G. *Inorg. Chim. Acta* **1988**, *147*, 77–85.

$E^{II/I} = 0.97[\sum E_L(L)] - 3.45$ but did not consider the $Fe^{II/I}$ couple.[85] The figure indicates that starting with Fe^{III} addition of the first electron yields Fe^{II} for > 1 $\sum E_L(L) < 3$; the second electron addition yields $Fe^{II}(bpy^{\bullet -})$ for > 1 $\sum E_L(L) < 2.7$, but Fe^{I} for $\sum E_L(L) > 2.7$. Points are shown for complexes **1**, **7**, and **2**, all of which are predicted to be reduced at bpy. Our observations indicate, however, that **1** and **2** are reduced at the metal. This disparity could simply reflect the inappropriateness of the $Fe^{II/I}$ data for the present system. However, it is possible that bpy is the initial reduction site but that intramolecular electron transfer (eq 6), followed by ligand dissociation (eqs 2 and 8) yields Fe^{I}, which is quickly reduced to Fe^0 (eqs 3 and 9).

$$M^N(bpy)L + e^- \rightleftharpoons [M^N(bpy^{\bullet -})L]^- \quad (6)$$

$$M^N(bpy^{\bullet -})L^- \rightleftharpoons [M^{N-1}(bpy)L]^- \quad (7)$$

$$[M^{N-1}(bpy)L]^- \rightleftharpoons [M^{N-1}(bpy)]^- + L \quad (8)$$

$$[M^{N-1}(bpy)]^- + e^- \rightarrow [M^{N-2}(bpy)]^{2-} \quad (9)$$

The reaction scheme of eqs 6−9 is prevalent in $Re^{I}(bpy)$ systems in which the intramolecular electron transfer is quite unfavorable.[86] Kaim has found such behavior for the case of $(C_6H_6)(bpy)MCl^+$ (M = Ru or Os) for which $\sum^5 E_L = 1.7$ V vs NHE, where L in eqs 6−8 is Cl^-.[87] Assuming that is $S_m \sim 1$ (eq 4), the key to predicting metal versus bpy reduction is knowledge of the magnitude of I_m for the $Ru^{II/I}$ couple. Lu et al. have estimated I_m values for the first transition series,[85] but at present, none are available for ruthenium. It is likely somewhat negative of the −3.3 value used above for iron.

In Table 4, we list the reactivity properties next to the proposed reduction site assignments. It is not obvious at this time how the initial reduction site influences the reactivity. The factors that determine the reduction sites in systems like these are not well understood or controlled, despite their critical importance to catalytic chemistry. In addition, the intramolecular processes that move electrons to/from ligand to metal (as in the transformation[67] of $Ru(bpy)_2(CO) + H_2O$ to $Ru(bpy)_2(CO)H^+ + OH^-$) merit study.

Concluding Remarks

In this paper, we report the structural, spectroscopic, and electrochemical properties of low-spin iron(II) complexes. We compare the properties and reactivities of previously prepared hydride complexes of iron(II) and ruthenium(II) with mixed phosphite and bpy ligand sets. Hydrides of both metals are reduced around −1.4 V vs AgCl/Ag in acetonitrile, but the reduction site varies with the metal, being the bpy ligand for the ruthenium hydride complexes but the metal itself for the iron hydride complex. Preliminary work indicates that the reduced hydride complexes react with CO_2, but the identity(ies) and yields of the carbon product(s) have not been established.

Acknowledgment. This research was carried out at Brookhaven National Laboratory under Contract DE-AC02-98CH10884 with the U.S. Department of Energy and supported by its Division of Chemical Sciences, Geosciences and Biosciences of the Office of Basic Energy Sciences. We thank Dr. Yasuo Matsubara for doing some of the MS measurements.

Supporting Information Available: Preparation and characterization of **7**−**9**, NMR spectra, UV−vis spectra, ESI-MS data, electrochemical results, comparisons of redox potentials with other complexes, details of the data collection and reduction, positional parameters and anisotropic thermal parameters for the non-hydrogen atoms, calculated positions for the hydrogen atoms, and a complete list of bond lengths and angles for **1**, **4**, **8**, and **9** as PDF files as well as in a CIF file. This material is available free of charge via the Internet at http://pubs.acs.org.

(85) Lu, S. X.; Strelets, V. V.; Ryan, M. F.; Pietro, W. J.; Lever, A. B. P. *Inorg. Chem.* **1996**, *35*, 1013–1023.
(86) Hayashi, S. K.; Brunschwig, B. S.; Fujita, E. *J. Am. Chem. Soc.* **2003**, *125*, 11976–11987.
(87) Kaim, W.; Reinhardt, R.; Sieger, M. *Inorg. Chem.* **1994**, *33*, 4453–4459.